Photonic Jet by a NearUnityRefractiveIndex Sphere on a Dielectric Substrate with High Index Contrast

Yue, Liyang; Yan, Bing; Monks, James; Dhama, Rakesh; Wang, Zengbo; Minin, Oleg; Minin, Igor

Annalen der Physik

DOI:
10.1002/andp.201800032

Published: 01/06/2018

Peer reviewed version

Article type: Original paper

Photonic jet by a near-unity-refractive-index sphere on a dielectric substrate with high index contrast

Liyang Yue[1,], Bing Yan[1], James N. Monks[1], Rakesh Dhama[1], Zengbo Wang[1], Oleg V. Minin[2], and Igor V. Minin[3,*]*

*Corresponding authors: E-mails: l.yue@bangor.ac.uk and prof.minin@gmail.com

[1]School of Electronic Engineering, Bangor University, Dean Street, Bangor, Gwynedd, LL57 1UT, UK
[2]National Research Tomsk State University, Lenin Ave., 36, Tomsk, 634050, Russia
[3]National Research Tomsk Polytechnic University, Lenin Ave., 30, Tomsk, 634050, Russia

Abstract

Photonic jet is normally generated in transmission mode representing as a spatially localized high-intensity region on the shadow side of a particle-lens with refractive index contrast of 1.3 - 1.7 to background medium illuminated by a plane wave. In this paper, a photonic jet in the opposite direction of plane wave propagation is discovered in the area above the upper boundary of a near-unity-refractive-index sphere on a high-refractive-index dielectric substrate. It is found that redistribution of power flows is inhibited during the process of reflected wave passing the near-unity-refractive-index sphere, which leads a unique effect that focus position and shape of the produced photonic jet in reflection mode can be maximally maintained in the vicinity of the sphere regardless of modulation of refractive index of the dielectric substrate material in a wide range. Best transverse dimension of the reflected photonic jet achieves 0.48 of wavelength of the incident plane wave.

1. Introduction

A photonic jet is a localised narrow, high-intensity, and weak-diverging focusing area in the near-field of the dielectric particle-lens illuminated by a plane wave. Many novel devices on the applications of imaging and sensing, such as high numerical aperture lens [1, 2], photonic

crystal/liquid lens [3-5], GRIN lens with subwavelength defect [6] and metalenses [7, 8], have been afforded based upon the aforementioned features of photonic jet. Photonic jet normally is created in transmission mode, which means it appears on the shadow side of a dielectric particle-lens and elongates into the free space in propagation direction of the plane wave. Refractive index contrast (particle to background media, usually 1.3 – 1.7) and scaling effect of the dielectric particle (relative-to-wavelength size) are two main factors that affect its formation [2, 9]. Also, it is known that almost all natural-solids have refractive indexes above 1.30, but the artificial near-unity-refractive-index materials, e.g. aerogel (refractive index 1.002 to 1.265) and aluminium oxide nanolattice film (refractive index 1.025), were developed to increase efficiency of ring-imaging Cherenkov detector (RICH) and photonic resonators in the last few years, respectively [10-12]. Recently Abdelrahman et al. studied broadband suppression of backscattering using a wavelength-sized low-index dielectric sphere [13]. However, to best of our knowledge, it has never been systematically investigated the photonic jet produced by the particle-lens made of near-unity-refractive-index material in reflection mode before.

Meanwhile, the ideal situation in transmission mode that particle-lens suspends in the air or a medium with a steady position is difficult to achieve in the experiment. Consequently, a particle-lens situated on a flat substrate is commonly used to establish an approximate model to research photonic jet in reality. Bobbert and Vlieger firstly used Mie theory to calculate reflection of dipole radiation to understand light scattering by a sphere on a substrate in 1986 referring to the problem of ‘Particle on Surface (POS)’ [14]. Hereafter Lilienfeld further developed this model and used it to optically detect particle contamination on a surface in the same year [15]. With the development of laser technology and material science, these initial achievements, including an analytical Mie theory model of particle on substrate and its

algorithm, were gradually applied to solve the practical problem of laser cleaning of material surface [16]. Luk'yanchuk et al. built the predictive models of three-dimensional temperature distribution and thermal deformation of substrate for laser cleaning of spherical particles [14], and then Zheng et al. experimentally verified the corresponding theories from various substrates and laser sources [17].

Thus, these POS models were gradually improved and had begun to apply to other specific manufacturing areas, e.g. repair of mirror degradation caused by particle contamination, construction of biosensors, and optical particle sizing [18]. Besides, Wang et al. discovered the sharper focus of photonic jet existing within the particle-substrate contact region of a gold 40-nm-thick film and developed this to the first super-resolution white-light nanoscope according to the reciprocity principle in 2011 [19, 20]. This effect was also used to affect the plasmonic field enhancement in a nanogap between a dielectric sphere and a metallic substrate for design of a novel plasmonic structures, which can be as effective as that made of all-metal, used for surface-enhanced Raman spectroscopy (SERS), fluorescence spectroscopy, and nonlinear optical spectroscopy [21].

Previous literatures reported photonic jets in reflection mode with wide-angle performance by the non-spherical particles on metallic substrates, notwithstanding part of particle where contacts to the substrate must be trimmed into a flat surface to make the reflected photonic jet localize out of the particle [22-25]. In this paper, we successfully produced a new photonic jet in reflection mode using high refractive index contrast between a near-unity-index spherical particle-lens and a high-index dielectric substrate via the numerical simulation. Position and shape of this type of photonic jet can be maximally maintained around the sphere boundary in the opposite direction of plane wave propagation, pairing with the numerous dielectric

substrates varying refractive indexes. This effect is different from the photonic jets in reflection mode reported before, and may be beneficial to many potential applications, e.g. improvement of signal collection for SERS [26] and near-field scanning optical microscope (NSOM) [27], because of high accessibility of the photonic jet on sphere top for the biomedical samples in liquid. Power flow distributions and contours were plotted to demonstrate the phenomenon. Profiles of power flow intensity, focus positions, and transverse dimensions of the produced photonic jets were calculated to explore its forming mechanism against a variety of refractive indexes for the dielectric substrate material.

2. Results and discussion

Current models were built in the commercial finite integral technique (FIT) software package – CST Microwave Studio© (CST). A plane wave of 248 nm wavelength (λ), which was polarised along *y* axis, propagated from +*z* to –*z* direction. Models were structured as a spherical particle-lens with diameter of 1 μm on a flat square substrate with side length of 1.6 μm and thickness of 0.1 μm (it is important to note that sphere contacts to substrate without gap). Also, a model of a single sphere without substrate support was created as the reference, which was verified by a FORTRAN programme to calculate the analytical Mie theory solution. Open boundary was assigned in *x* and *y* directions, and open add space (air) boundary was along *z* axis, as shown in **Figure 1**. Refractive index of spherical particle-lens material, n_p, was set to constant 1.16 to mimic aerogel material and tune position of the reflected photonic jet to the upper boundary of the sphere against multiple reflective indexes of dielectric substrate, n_s, in this study. Models were discretized by the default hexahedral mesh using the perfect boundary approximation (PBA) method. Smallest and largest edges of the meshes were 5.26 nm and 20.86 nm, respectively. Meshes with the largest edges were only used for meshing of the add-space of the background media – air, and did not connect to the established meshes of the sphere

and substrate (did not surround the structure). Mesh size of 10 meshes (cells) per wavelength was adopted for the high-accuracy time domain solver in CST after a long-term meshing test to balance model accuracy and calculation time. Amplitudes of power flow (Poynting vector) shown in this paper were normalized to that for the incident plane wave in the air under the same boundary conditions. In CST, this process is based on the standard input electric field (E-field) intensity of the plane wave, E_0 = 1, and the corresponding magnetic field (H-field) intensity with a coefficient of $\sqrt{\frac{\varepsilon_0}{\mu_0}}$, where ε_0 and μ_0 are the electric constant and the magnetic constant, respectively.

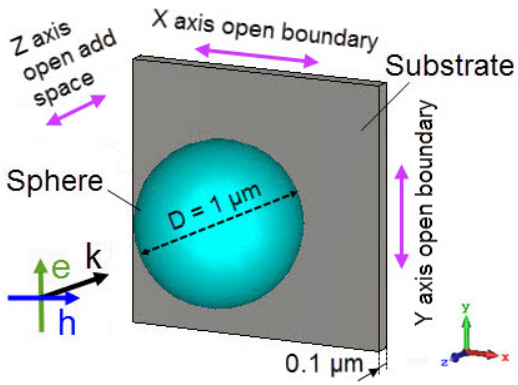

Figure 1. Diagram of CST model with the dimensions

Figure 2 illustrates power flow distributions (i) and contours (ii) in *yz* plane for the models of a single sphere with n_p = 1.16 without substrate (a) and the same spheres on the dielectric substrates with n_s = 2.58 (b), 2.77 (c), and 3.96 (d), respectively. Figure 2 (a) i and ii show a typical photonic jet in transmission mode formed on the shadow side of the sphere which acts as a refractive micro-lens to focus the incident light wave within a small volume. This result was verified by the analytical solution calculated by Mie theory, as shown in **Figure S1**. The key features of two figures, such as the jet shape and position, existence of a low-intensity area at lower boundary, and distribution of power flow intensity, well match each other and demonstrate the same tendency of particle-lens focusing. In Figure 2 (b) i, there is a circular

hotspot (yellow colour) on top of the sphere supported by a dielectric substrate with n_s = 2.58, but no typical jet shape is formed. Majority of power flows penetrate the sphere and substrate, which leads a high-intensity area below the substrate. The corresponding contour of power flow vectors in Figure 2 (b) ii highlight two vortexes that are close to each other at the centre of the sphere. It is known that power flows normally couple to the other planes through the singularities in these vortexes [28]. This causes the low-intensity region at sphere centre and terminates stream of the reflected power flows to pass the sphere.

By contrast, the dielectric substrates with larger refractive index, such as substrates with n_s = 2.77 and 3.96 in Figure 2 (c) and (d) respectively, are able to provide higher reflectance, *R*, at interface between sphere and the flat surface based on the simplified Fresnel equation, which is given by [29],

$$R = \left(\frac{n_p - n_s}{n_p + n_s}\right)^2 \quad (1)$$

From equation (1), it is known that strong reflectance, *R*, should be induced by a large numerator in the equation (1), which is equivalent to a huge different value between n_p and n_s. For this reason, photonic jets on top of spheres pairing with the penetrative high-intensity areas can be found in both Figure 2 (c) and (d). Morphologies of two photonic jets shown in these two figures are extremely similar despite the enormous differences between their n_s and peak intensities indicated in colour ramps. In Figure 2 (c) i and (d) i, the reflected photonic jets represent the region possessing the highest intensity where precisely covers the sphere top and simultaneously initialize two ‘wings’ by sides that encounter the incident downward-light. Meanwhile, contours in Figure 2 (c) ii and (d) ii manifest that the produced photonic jet stems from an upwards high-intensity stream of power flows reflected by the dielectric substrates with larger n_s. This stream separates the two vortexes at the sphere centre and diverges at the end of

the photonic jet characterizing as the ‘wing’ shape. It is noted that all power flows entering flanks of the sphere are from the diverged ‘wings’ and the incident power flow by sides, which complete two power flow circulations in the sphere and its vicinity. Power flows could circulate the near-field area of the sphere multiple rounds according these phase trajectories rather than normal one-time penetration [30]. It is suggested that this mechanism may effectively enhance intensity of the photonic jet and weaken the influence of redistribution of power flow on a photonic jet. Besides, it is found that morphology of the photonic jet generated by dielectric sphere and substrate with the high index contrast is highly similar to that from the model with an aluminium substrate (Al, n_s = 0.17, extinction coefficient, k = 2.83 [31]) under the identical simulation conditions, as shown in Figure 2 (e). In Figure 2 (e), modulation of the photonic jet caused by standing wave is clearly visible. Luk’yanchuk et al. analytically studied focusing of a dielectric particle on a metallic substrate with a nano-gap before [32]. But their calculation did not involve any spheres made of the near-unity-refractive index materials, also calculation of the intensity distribution inside the spheres was not mentioned in that paper.

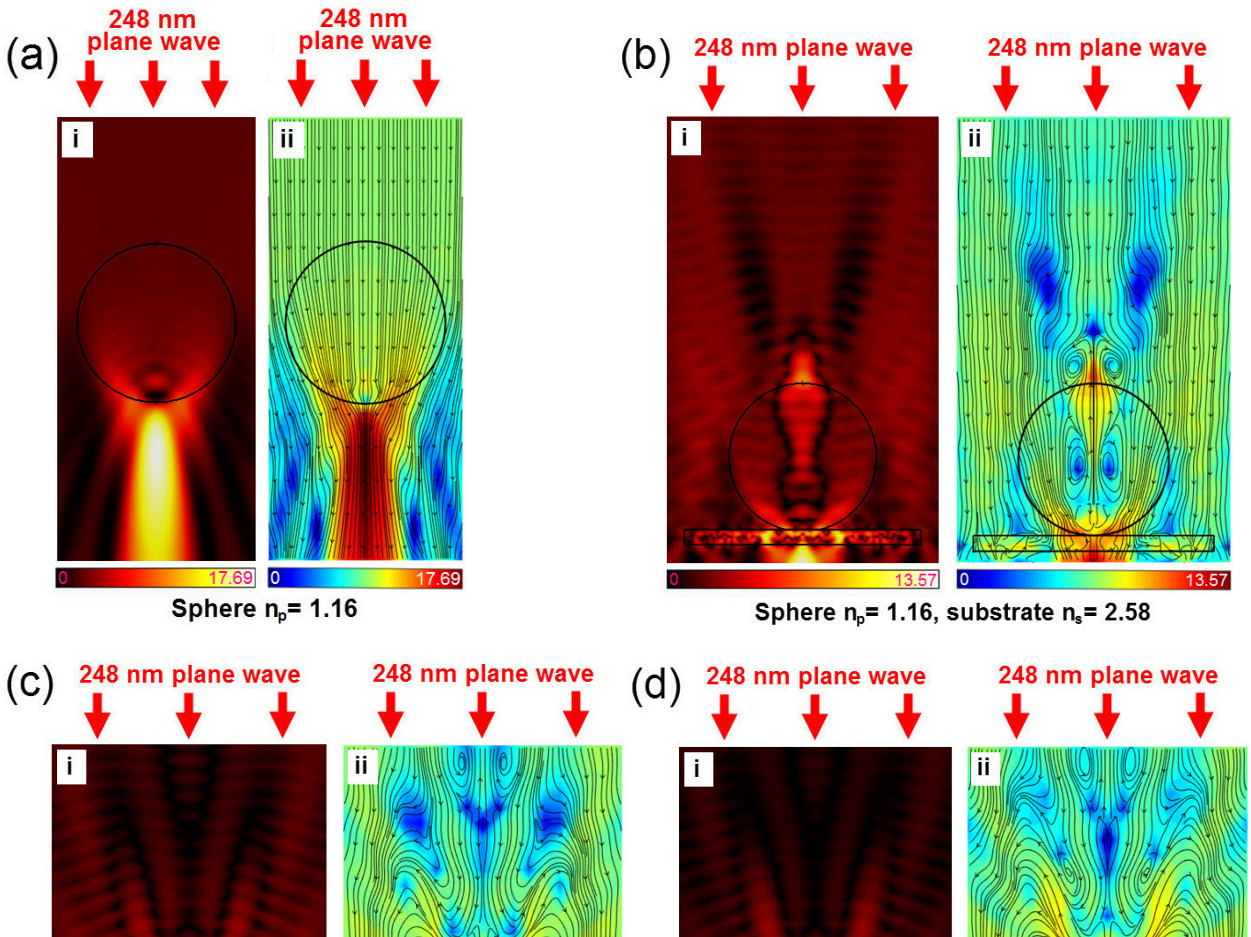

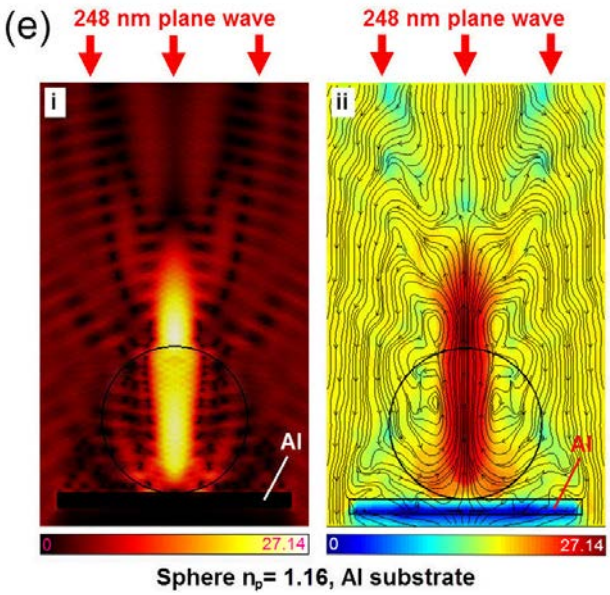

Figure 2. Power flow distributions (i) and contours (ii) in *yz* plane for models of a single sphere with n_p = 1.16 (a) and the same spheres on dielectric substrates with n = 2.58 (b), 2.77 (c), and 3.96 (d), and aluminium substrate (e), respectively.

Relying on the spherical particle-lens with the same n_p = 1.16, photonic jet in reflection mode can be generated and geographically maintained in a small area near the upper boundary of the sphere against the dielectric substrates with a wide range of n_s, as examples shown in Figure 2 (c) and (d). **Figure 3** (a) demonstrates *z* direction profiles of power flow intensity along the

central axis of the sphere (x = 0, y = 0) for models of substrates with n_s ranging from 2.77 to 4.76 (curves indicated in legend). The incident plane wave propagates from +z to -z direction, which is marked as a red arrow from right to left in Figure 3 (a). Spherical particle-lens with 1 μm diameter occupies the space from z = 1000 to z = 0 (indicated as 'sphere' zone in Figure 3 (a)) that is in front of the substrate zone from z = 0 to z = -100 (indicated as 'substrate' zone in Figure 3 (a)). Figure 3 (a) clearly indicates that most of focus positions of the produced photonic jets (position where highest power flow intensity is) concentrate in a narrow area which is only about 30 nm wide and border on the sphere boundary (indicated as 'focus area' in Figure 3 (a)). Curves of n_s = 3.56, 3.70, and 4.76, behave a different tendency which exhibits the relatively low peaks in the focus area compared to those of other curves in the same zone and even their own peaks in the sphere space. Meanwhile, it is found that power flow enhancement of the reflected jet is significantly related to the magnitude of n_s. The normalized power flow amplitude can maximally be 32.15 for the model of n_s = 4.32, but drops to only 2.95 for the model of n_s = 3.70, as shown in Figure 3 (a).

First row of Figure 3 (b) summarizes all focus positions presented in Figure 3 (a) against the n_s values. It is shown that all focuses stabilize around the position of z = 1030 nm (marked as a red dashed line in first row of Figure 3 (a)) except ones for ns = 3.56 and 4.76. Regions of the high-amplitude power flow localization were manifested in our preliminary simulations of the spheres with n_p ranges from 1.3 to 1.7 on both dielectric and metallic substrates, as shown in the examples of models with spheres n_p = 1.36, 1.46, and 1.66 on the aluminium and n_s = 3.96 dielectric substrates respectively in **Figure S2**. An overall tendency is summarized as movement of the reflected photonic jet toward the interior of the particle with increase of n_p. But these high-amplitude regions cannot be claimed as the high-quality photonic jets in reflection mode because of poor accessibility inside the particles for the potential applications.

By comparison, the near-unity-refractive-index sphere with n_p = 1.16 can 'fix' the reflected photonic jet to the area just over the upper boundary of the sphere on dielectric substrates with the varying n_s, as shown in Figure 3 (a). n_s is limited to no more than 5.0 in this study as reality of natural elements.

Besides, transverse dimensions (full width at half maximum, FWHM) of the reflected photonic jets by dielectric sphere and substrate simulated in this study are shown in second row of Figure 3 (b). In fact, all FWHMs in second row of Figure 3 (b) are far shorter than those for the models of transmission mode, as shown in Figure 2 (a) (FWHM = 183 nm = 0.74λ), and aluminium substrate, as shown in Figure 2 (e) (FWHM = 164 nm = 0.66λ), but only dimension of n_s = 4.76 can be beyond diffraction limit (DL) of air - $\lambda/2$ = 124 nm, which is displayed as a black dashed line in second row of Figure 3 (b), due to a focus outside of the particle (z = 1003). It is noted that photonic jets in transmission mode shown in Figure 2 (a) (numerical solution) and Figure S1 (analytical solution) both behave the weak focusing caused by the low contrast of refractive index (particle to air, 1.16:1), which results in that their transverse dimensions cannot overcome DL. The *y* direction profiles of power flow at focus for models of aluminium substrate (z = 1081.8, x = 0) and dielectric substrates with n_s = 4.32 (z = 1029.2, x = 0) and 4.76 (z = 1003, x =0) are shown in Figure 3 (c). Profile of photonic jet reflected by an aluminium substrate (black curve in Figure 3 (c)) has a sharper tip compared to the round ones for models with dielectric substrate, and its FWHM (164 nm = 0.66λ) is much longer than those of the dielectric substrate models shown in the same figure (n_s = 4.32 red curve: FWHM = 133 nm = 0.54λ, n_s = 4.76 blue curve: FWHM = 120 nm = 0.48λ). Profile of the model containing the dielectric substrate with n_s = 4.32 (red curve in Figure 3 (c)) demonstrates a higher peak enhancement of power flow (normalized amplitude 32.15) than that for aluminium substrate model (normalized amplitude 27.14). However, the photonic jet produced by the dielectric substrate with n_s = 4.76, as the

only one with super-resolution transverse dimension (FWHM = 120 nm = 0.48λ), delivers a low peak of normalized power flow amplitude achieving 8.55. Therefore, Figure 3 indicates that focuses of the models with various n_s all concentrate in a small area around the position of z = 1030 nm, and a dielectric substrate with a large n_s is able to further reduce the FWHM of a reflected photonic jet compared to that for the same sphere on an aluminium substrate, although only FWHM of the n_s = 4.76 model can overcome the diffraction limit in the air.

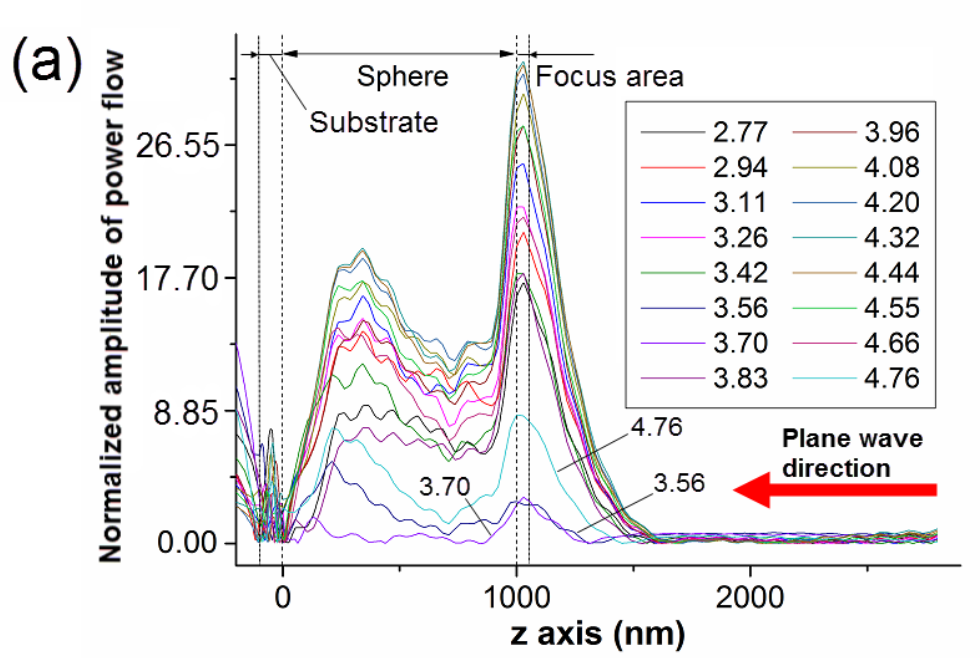

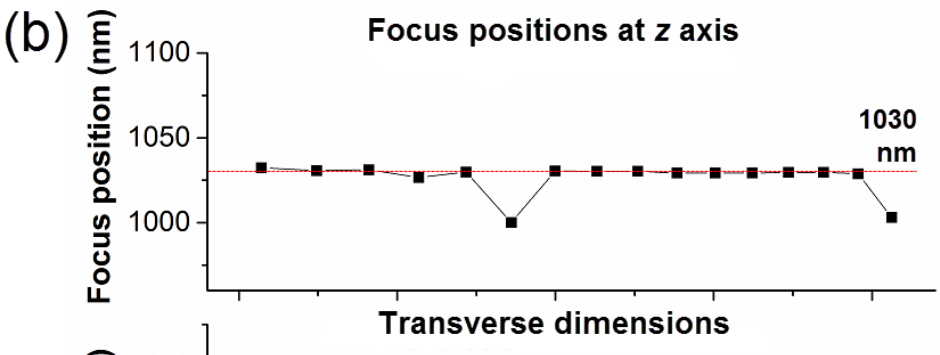

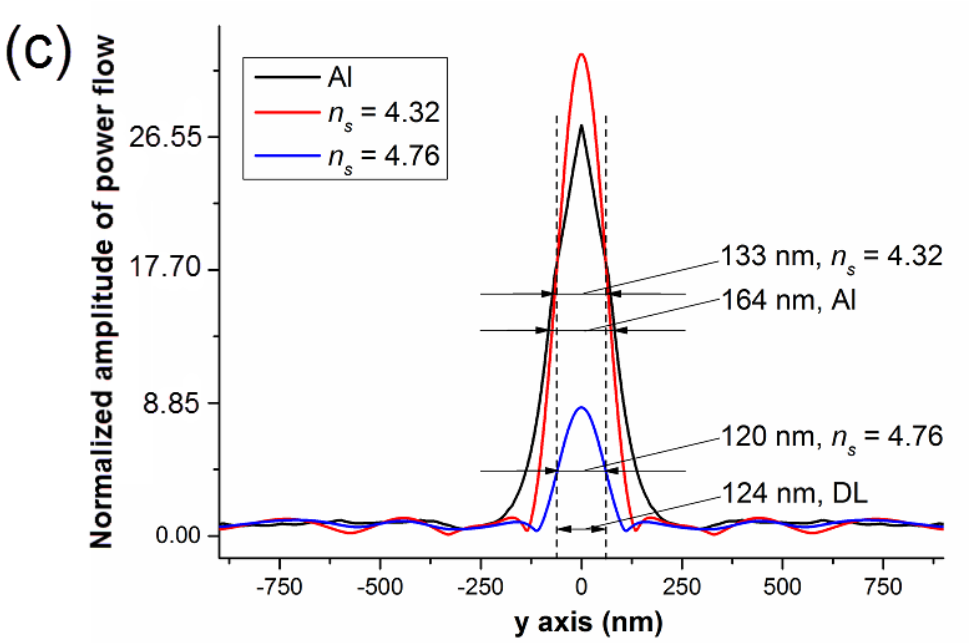

Figure 3. (a) *z* direction profiles of power flow along the central axis of the sphere in models of dielectric substrates with n_s ranging from 2.77 to 4.76 (b) Focus positions at *z* axis (first row) and transverse dimensions (second row) for the reflected photonic jets (c) The *y* direction profiles of power flow at focus for models of aluminium substrate and dielectric substrates with n_s = 4.32 and 4.76, respectively.

3. Conclusion

The new type of photonic jet in reflection mode was achieved via the numerical simulation of a near-unity-refractive-index spherical particle-lens situated on a flat dielectric substrate with high index contrast under vertical light illumination. It is shown that position and shape of the reflected photonic jet can be maximally maintained in an area over the upper boundary of the sphere on the dielectric substrates with a wide range of refractive indexes. Power flow analysis suggests that this phenomenon could be attributed to reflectance increase caused by refractive index contrast and the consequent multi-round power flow circulations in the sphere and its vicinity. This result may be of interest for the imaging/sensing applications, e.g. construction of biosensors, optical particle sizing, and super-resolution optical microscopy in reflection mode, also could improve field magnification and impedance matching of a photonic device, e.g. coupling more energy in/out of the device.

Acknowledgements

The authors gratefully acknowledge the financial support provided by Sêr Cymru National Research Network in Advanced Engineering and Materials (NRNF66 and NRN113), the Knowledge Economy Skills Scholarships (KESS 2, BUK289), and within the framework of Tomsk Polytechnic University Competitiveness Enhancement Program.

Received: ((will be filled in by the editorial staff))
Revised: ((will be filled in by the editorial staff))
Published online: ((will be filled in by the editorial staff))

Key words: refractive-index-contrast; particle-lens; scattering; near-field optics;

References

[1] S. M. Mansfield, W. R. Studenmund, G. S. Kino, and K. Osato, *Opt. Lett.* **18**, 305-307 (1993).

[2] I. V. Minin, and O. V. Minin, *Diffractive optics and nanophotonics: Resolution below the diffraction limit*. (Springer, Berlin, Germany, 2016).

[3] I. V. Minin, O. V. Minin, Y. R. Triandaphilov, V. V. Kotlyar, *Opt. Mem. Neural Networks* **17**, 244-248 (2008).

[4] G. Xiong, G. Han, C. Sun, H. Xu, H. Wei, and Z. Gu, *Adv. Funct. Mater* **19**, 1082 (2009).

[5] G. Xiong, Y. Han, C. Sun, L. Sun, G. Han, and Z. Gu, *Appl. Phys. Lett.* **92**, 241119 (2008).

[6] Y. Li, Y. Fu, O. V. Minin, and I. V. Minin, *Opt. Mater. Express* **6**, 2628 (2016).

[7] M. Kim, and J. Rho, *Nano Converg.* **2**, 22 (2015).

[8] N. Yu, and F. Capasso, *Nat. Mater.* **13**, 139-150 (2014).

[9] B. S. Luk'yanchuk, R. Paniagua-Dominguez, I. V. Minin, O. V. Minin, and Z. B. Wang, *Opt. Mater. Express* **7**, 1820-1847 (2017).

[10] A. Yu. Barnyakov, M. Yu. Barnyakov, V. S. Bobrovnikov, A. R. Buzykaev, A. F. Danilyuk, V. L. Kirillov, S. A. Kononov, E. A. Kravchenko, A. P. Onuchin, *Nucl. Instrum. Methods Phys. Res. A* **553**, 70-75 (2005).

[11] X. A. Zhang, A. Bagal, E. C. Dandley, J. Zhao, C. J. Oldham, B. I. Wu, G. N. Parsons, C. H. Chang, *Adv. Funct. Mater.* **25**, 6644 (2015).

[12] M. Tabata, I. Adachi, T. Fukushima, H. Kawai, H. Kishimoto, A. Kuratani, H. Nakayama, S. Nishida, T. Noguchi, K. Okudaira, Y. Tajima, H. Yano, H. Yokogawa, H. Yoshida, "Development of silica aerogel with any density", 2005 IEEE Nuclear Science Symposium - Conference Record. Vol. 2., Puerto Rico (2005).

[13] M. Ismail Abdelrahman, C. Rockstuhl, and I. Fernandez-Corbaton, *Sci. Rep.* **7**, 14762 (2017).

[14] P. A. Bobbert, and J. Vlieger, *Physica A* **137**, 209-242 (1986).

[15] P. Lilienfeld, *Aerosol Sci. Tech.* **5**, 145-165 (1986).

[16] B. S. Luk'yanchuk, Y. W. Zheng, and Y. F. Lu, *Proc. SPIE* **4065**, 576 (2000).

[17] Y. W. Zheng, B. S. Luk'yanchuk, Y. F. Lu, W. D. Song, and Z. H. Mai, *J. Appl. Phys.* **90**, 2135-2142 (2001).

[18] F. Moreno, J. M. Saiz, and F. Gonzalez, Light scattering by particles on substrates. Theory and Experiments, In: A. A. Maradudin (Ed.) *Light scattering and nanoscale surface roughness.* (Springer, Boston, USA, 2007).

[19] Z. B. Wang, W. Guo, L. Li, B. Luk'yanchuk, A. Khan, Z. Liu, Z. Chen, and M. Hong, *Nat. Commun.* **2**, 218 (2011).

[20] R. J. Potton, *Rep. Prog. Phys.* **67**, 717 (2004).

[21] T. Hutter, F. M. Huang, S. Elliot, and S. Mahajan, *J. Phys. Chem. C* **117**, 7784 (2013).

[22] I. V. Minin, O. V. Minin, V. Pacheco-Peña, and M. Beruete, *Opt. Lett.* **40**, 2329 (2015).

[23] I. V. Minin, O. V. Minin, and I. S. Nefedov, *Opt. Lett.* **41**, 785 (2016).

[24] I. V. Minin, O. V. Minin, V. Pacheco-Peña, M. Beruete, *Quantum electron.* **46**, 555 (2016).

[25] I. V. Minin, O. V. Minin, N. A. Kharitoshin, Proc. of the 16th Int. conf. on Micro/Nanotechnologies and Electron Devices (EDM 2015), Novosibirsk (2015).

[26] I. Alessandri, and J. R. Lombardi, *Chem. Rev.* **116**,14921 (2016).

[27] J. Kerimo, M. Büchler, and W. H. Smyr, *Ultramicroscopy* **84**, 127 (2000).

[28] Z. B. Wang, B. S. Luk'yanchuk, M. H. Hong, Y. Lin, and T. C. Chong, *Phys. Rev. B* **70**, 035418 (2004).

[29] M. Born, and E. Wolf, *Principles of optics: Electromagnetic theory of propagation, interference and diffraction of light, 7th Ed.* (Cambridge University Press, Cambridge, UK, 1999).

[30] M.V. Bashevoy, V. A. Fedotov, N. I. Zheludev, *Opt. Expr.* **13**, 8372 (2005).

[31] A. D. Rakić, A. B. Djurišic, J. M. Elazar, and M. L. Majewski, *Appl. Opt.* **37**, 5271 (1998).

[32] B. S. Luk'yanchuk, Z. B. Wang, W. D. Song, and M. H. Hong, *Appl. Phys. A* **79**, 747 (2004).